Evidence of electron-phonon and spin-phonon couplings at the Verwey transition in Fe_3O_4

Ankit Kumar,[1] Sujeet Chaudhary,[1] Dinesh K. Pandya,[1,*] and Shiv K. Sharma[2]
[1]*Thin Film Laboratory, Department of Physics, Indian Institute of Technology Delhi, New Delhi 110016, India*
[2]*Hawai'i Institute of Geophysics and Planetology, University of Hawai'i, Honolulu, Hawai'i 96822, USA*
(Received 30 September 2013; revised manuscript received 2 June 2014; published 3 July 2014)

Using low temperature Raman spectra on two-dimensional epitaxial Fe_3O_4 thin films, the presence of electron-phonon (e-p) and spin-phonon (s-p) couplings is established in the vicinity of Verwey transition (T_V). The e-p coupling is linked to A_{1g} and T_{2g} Raman modes and s-p to the T_{2g} mode, below isotropic point (T_K). The parabolic dependence of the characteristic spin-correlation eigenstates on the magnetization, $\Delta\omega_{s-\mathrm{phn}} \propto \langle S_i|S_J\rangle \propto [\frac{M(T)}{M_S}]^2$ observed between T_K and T_V demonstrates the presence of s-p coupling. This work provides experimental evidence of the onset of correlation between these couplings and charge-orbital ordering below T_K to govern the Verwey transition in Fe_3O_4 films.

DOI: 10.1103/PhysRevB.90.024302 PACS number(s): 78.30.Er, 78.20.Ls, 78.66.Bz, 78.68.+m

I. INTRODUCTION

One of the most interesting physical phenomena associated with Fe_3O_4 (magnetite) crystals is the occurrence of metal-insulator (MI) transition at ~120 K (T_V), the so-called Verwey transition (VT) [1,2]. The Fe_3O_4 also undergoes a change in the magnetic anisotropy behavior in the form of easy-axis changing from [111] to [100] at the isotropic-point temperature (spin reorientation temperature), $T_K = 135$ K [3,4]. Both the T_K and T_V are highly sensitive to the presence of antiferromagnetic (AF) defects, and the inherence of these defects often ceases these transitions [5]. VT is accompanied by the change in crystal symmetry from cubic to rhombohedrally distorted monoclinic phase and is confederated with the aberrance in most physical properties of Fe_3O_4, e.g., a giant increase in resistivity and sudden drop in magnetization [2]. Despite intensive investigations over a half-century, the origin of VT continues to be elusive and is an arguable issue of fundamental understanding. Verwey originally described this transition as a disorder-order transition [6] and suggested that the Coulomb repulsion between neighboring cations (Fe^{2+} and Fe^{3+}) at the octahedral sublattice sites organizes them on the alternate (100) planes, which lead to the crystal distortion. The reduction in the conductivity below T_V as a consequence of the ionic or charge ordering was also suggested. Later, Anderson [7] suggested the importance of short range order in VT, due to the Coulomb interaction between cations at octahedral sites, in order to minimize the electrostatic energy. However, in Anderson's model, the abrupt change in conductivity around T_V is not expected. The inconsistency with Anderson's model is understandable as both the elastic and the Coulomb energies should be minimized rather than Coulomb energy alone.

Further, Ihle and Lorenz [8] pointed out the importance of strong coupling of interatomic Coulomb interaction to lattice at VT. Later, based on theoretical calculations employing generalized gradient approximations under onsite Coulomb interactions, it was proposed that the charge-orbital (CO) ordering, and therefore VT, is driven by Fe $3d$-electron correlations [9]. The CO observed in Fe_3O_4 is consistent with the x-ray and inelastic neutron scattering (INS) and entropy measurements [4,9,10]. The presence of strong onsite Coulomb interactions amplifies the conduction electron coupling to the phonon ordering parameter below T_V, and it assists in VT [10]. Later, using three different results including *ab initio* calculations, Hoesch *et al.* [11] found that the electron-phonon (e-p) coupling of the Fe $3d$-electrons stabilizes the CO that drives the change in crystal symmetry at T_V, and this e-p coupling also induces the strong phonon-anharmonicity. However, the range of temperature over which phonon-anharmonicity dominates and the role of T_K and its correlation with the e-p and spin-phonon (s-p) coupling (novel and vital aspect for VT) are still obscure and need to be enlightened by experimental verification, as their consideration is inevitable in governing the occurrence of VT. Isothermal Raman measurements offer a powerful tool to probe such issues.

Previously, low temperature Raman measurements on bulk Fe_3O_4 have been reported to understand whether the electronic and phononic states are acting together near VT [2,12–14]. But the invisibility of T_K and laconism about the existence of e-p and s-p couplings persisted. The invisibility of T_K is because of (i) use of insensitive Raman A_{1g} mode peak [13] instead of highly sensitive T_{2g} mode peak for temperature-dependent studies, (ii) use of sparse data points in the vicinity of T_V and T_K [12–14], and (iii) use of antiphase boundary (APB) dominated samples, e.g., thin films grown on MgO or Al_2O_3 [15–17] surface-treated single crystals [14]. It has been reported that the occurrence of T_K vanishes/broadens in the presence of a high density of APBs, as T_K is highly sensitive to AF disorders [5]. APBs/AF couplings exist in films grown on MgO and Al_2O_3 substrates, and surface treatment generates the AF couplings or highly effects the line-shape parameters [16–18]. Therefore, the presence of AF coupling diminished the appearance of phonon anharmonicity and T_K in all of these studies. Thus, we believe that inconsistencies in previous works are associated either with poor sample quality or inappropriate measurements, and it then becomes hard to probe the role of strong e-p and s-p interactions around T_V.

Despite Raman studies, *ab initio* calculations, INS, and resonant x-ray scattering [2,9–14], clear evidence of strong e-p and s-p interactions in the vicinity of T_V has yet to be established. McQueeney *et al.* [19] suggested the possibility of the presence of large s-p coupling in Fe_3O_4 below VT, but this claim needs pellucidity. In this paper, we report Raman measurements in the 90–295 K temperature range to enlighten the existence of phonon anharmonicity, e-p, and s-p

*Corresponding author: dkpandya@physics.iitd.ac.in

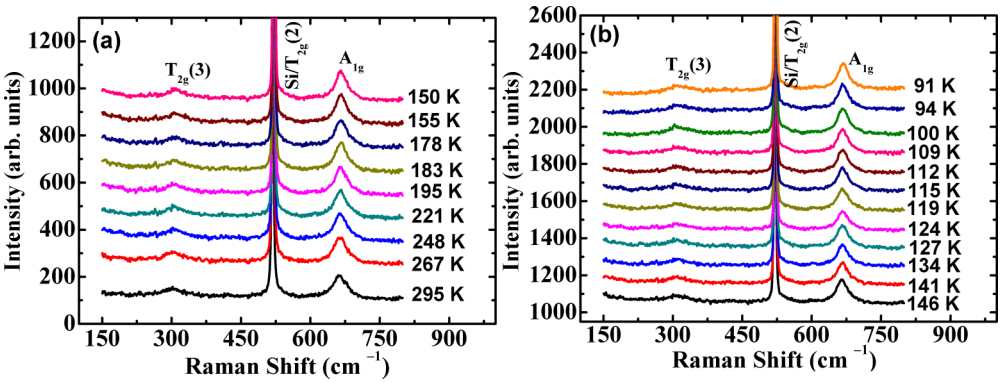

FIG. 1. (Color online) Raman spectra recorded in 150–800 cm^{-1} frequency range at some representative temperatures.

couplings. The work clearly demonstrates the existence of phonon anharmonicity down to $\sim T_K$ and the strong e-p and s-p couplings below $\sim T_K$.

II. EXPERIMENTAL DETAILS

High quality, stain free, APBs free and smooth (for enhanced Raman signal) layer-by-layer grown two-dimensional (2D) epitaxial Fe_3O_4 thin film sample grown at 600 °C [5] is chosen for the Raman measurements. Already reported [5] measurements on the same sample, like dM/dT in zero-field cooled–field cooled (ZFC-FC) protocol, magnetization vs field (M-H), etc., lend support to their excellent magnetic, electronic, and structural quality. Raman measurements were done using the Spex-Triplemate spectrometer and cooled (−80 °C) with a charge-coupled device (CCD) camera-based micro-Raman system with a temperature accuracy of ±2K [20,21]. A 514.5 nm Ar^+ laser at 5 mW power with a 20 × objective was used to record the Raman spectra in 180° scattering geometry. The polarized micro-Raman spectroscopic measurements were also performed at 300 K to establish the mode's symmetry and monocrystallinty of the sample.

III. RESULTS AND DISCUSSION

The Raman spectra in the 150–800 cm^{-1} frequency range at some representative temperatures are shown in Figs. 1(a) and 1(b). Only the strongest A_{1g}, $T_{2g}(2)$, and $T_{2g}(3)$ modes of Fe_3O_4 are observed down to the vicinity of VT. The positions of $T_{2g}(2)$ and $T_{2g}(3)$ modes of Fe_3O_4 coincide with that in Si. However, before acquiring temperature-dependent Raman spectra on Fe_3O_4, the optimizations of Raman laser power and recording time were performed on TiN/Si(100) to debar Si second-order Raman mode at $T_{2g}(3)$ mode position of Fe_3O_4. It may also be noted here that none of the Raman modes of TiN are seen due to its small thickness (8 nm). We therefore chose only A_{1g} and $T_{2g}(3)$ modes for analysis. For clarity and conciseness, the Raman spectra at 295, 150, and 91 K temperatures along with TiN/Si(100) buffered substrate is also shown in Fig. 2. Whereas Fig. 3 shows the portions of Raman spectra, highlighting the A_{1g} and $T_{2g}(3)$ modes, which are characterized by Γ_1^+, and Γ_5^+ irreducible representative symmetry operators [10], recorded at three different temperatures. Below T_V, each of the T_{2g} mode splits into three levels (i.e., B_{1g}, B_{2g}, and B_{3g}), but the A_{1g} mode of the high temperature cubic phase continues to exhibit the same vibrational symmetry below T_V. Verble *et al.* [2] assigned the A_{1g} mode to the diagonally symmetric stretching vibrations and the T_{2g} mode to the asymmetric and symmetric bending of oxygen with respect to the Fe ion [22]. To get the precise value of Raman line-shape parameters, the Raman spectra are fitted by convolution (multiplication) of Lorentzian and Gaussian functions to obtain minimum chi-square value, and backgrounds are subtracted by a second-order polynomial to get the more precise value of Raman line-shape parameters (Appendix A). The temperature dependence of the observed line width (Γ) and frequency (ω) of both modes are shown in Fig. 4. Both $\omega(T)$ and $\Gamma(T)$ highlight the occurrence of T_K and T_V, which is analogous to the dM/dT response of this sample [Fig. 5(c) of Ref. 5]. Therefore, in the following, we discuss the temperature dependence of the Γ and ω of A_{1g} and $T_{2g}(3)$ modes (Fig. 4) in terms of phonon-phonon (anharmonic), e-p and s-p coupling contributions to understand the VT.

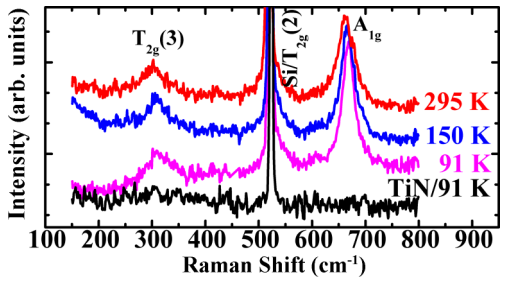

FIG. 2. (Color online) Raman spectra recorded in 150–800 cm^{-1} frequency range at 295, 150, and 91 K along with TiN(200)-buffered Si(100) substrate spectra at 91 K.

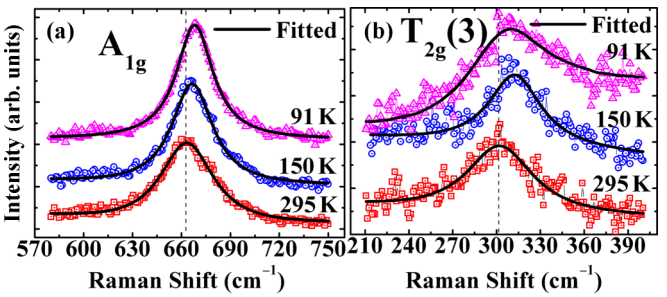

FIG. 3. (Color online) Raman spectra recorded at three temperatures and their line fits for (a) A_{1g} and (b) $T_{2g}(3)$ modes.

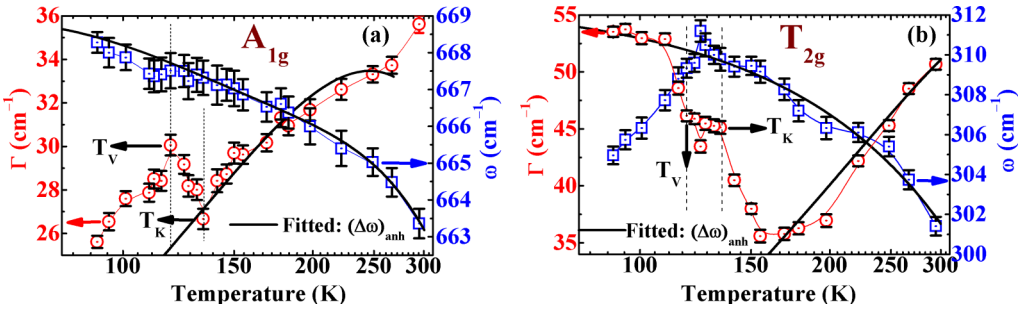

FIG. 4. (Color online) Temperature dependence of ω and Γ and their fitting using the anharmonic model for (a) A_{1g} and (b) $T_{2g}(3)$ modes.

As s-p interactions are expected to be much weaker at higher temperature, these could be ignored in Fe_3O_4 spectra taken above T_K. The frequency change of the ith phonon mode down to the vicinity of T_K in Fe_3O_4 can be described by

$$\Delta\omega = \omega_i(T) - \omega_i(0) = (\Delta\omega_i)_{\text{latt}} + (\Delta\omega_i)_{\text{anh}}, \tag{1}$$

where $\omega_i(0)$ is harmonic frequency. The quasiharmonic $(\Delta\omega_i)_{\text{latt}}$ term is governed by the modification of ionic binding energy due to distortion in lattice and is usually approximated by Gruneisen law as $(\Delta\omega_i)_{\text{latt}} = -\gamma_i \frac{\Delta V}{V}$, where γ_i is the Gruneisen parameter and $\frac{\Delta V}{V}$ is the fractional volume change [23,24]. INS studies on Fe_3O_4 demonstrated the compression of the unit-cell volume by 0.1% as temperature is reduced to T_V [25]. Therefore, its contribution cannot account for the observed changes in $\omega(T)$. The $(\Delta\omega_i)_{\text{anh}}$ term is intrinsic in nature and accounts for purely anharmonic effects due to thermal expansion. The contribution of the anharmonicity into phonon line width and frequency are investigated as a function of temperature using [26]

$$(\Delta\omega_i)_{\text{anh}} = \omega(T) - \omega(0) = A\left(1 + \frac{2}{e^x - 1}\right) + B\left(1 + \frac{3}{e^y - 1} + \frac{3}{e^y - 1^2}\right) \tag{2}$$

$$\Gamma(T) = C\left(1 + \frac{2}{e^x - 1}\right) + D\left(1 + \frac{3}{e^y - 1} + \frac{3}{e^y - 1^2}\right), \tag{3}$$

where $x = \hbar\omega_0/(2k_BT)$ and $y = \hbar\omega_0/(3k_BT)$, ω_0 is the characteristic frequency of the mode, and A, B, C, and D are constants. $\omega(T)$, $\omega(0)$ and $\Gamma(T)$, $\Gamma(0)$ are the frequency and line widths at T and 0 K, respectively. In each equation, while the first term is associated with the "three-phonon process," i.e., decay of anharmonic phonon into two equal energy acoustical phonons, the second term is associated with the four-phonon process ($\omega_1 = \omega_2 = \omega_3 = \frac{\omega_0}{3}$). Both anharmonic equations of $\omega(T)$ and $\Gamma(T)$ comprise the same third- and fourth-order phonon terms; therefore, in both $\omega(T)$ and $\Gamma(T)$ the mode anharmonicty is expected to go down to the same temperature. Figure 4(a) clearly depicts the best anharmonic fitting for $\omega(T)$ and $\Gamma(T)$ data down to T_K for A_{1g} mode. The fitted values of A, B, C, and D are -0.146, -0.039, 13.30, and -0.790, along with $669 = \omega_0$. Similarly, Fig. 4(b) shows the best-fit curves (anharmonic behavior) down to 150 K for ω and Γ corresponding to the T_{2g} mode. The fitted values of parameters A, B, C, and D are -0.246, -0.016, 4.676, and -0.0574, along with $316 = \omega_0$. In both modes, the values of constant parameter "D" linked to the four-phonon anharmonic process is quite small. Therefore, the line-shape parameters of A_{1g} and T_{2g} modes are clearly dominated by the cubic anharmonic behavior down to T_K and 150 K, respectively, though the anharmonic fit curves are extrapolated down to 91 K in $\omega(T)$. However, below $\sim T_K$ to T_V, the sharp rise is observed in $\Gamma(T)$ and a modest increase in $\omega(T)$, as shown in Fig. 4. Only the e-p coupling strongly contributes in line width (e-p $\propto \Gamma$) and negligibly in frequency (e-p $\propto \frac{1}{\omega^2}$) [27], whereas it is vice versa for s-p coupling. Therefore the increase in $\Gamma(T)$ for both the modes below T_K could be dominated by e-p coupling. However, compared to the A_{1g} mode, the T_{2g} modes are highly sensitive to electronic and magnetic exchange interactions [14]. Therefore, large changes that abound in $\Gamma(T)$ and $\omega(T)$ of the T_{2g} mode can be directly linked to the significant presence of such exchange interactions. As discussed above, anharmonic terms only govern the line-shape parameters down to $\sim T_K$; the e-p and s-p couplings (discussed in next sections) are therefore expected to provide significant contribution to the line-shape parameters below T_K.

To explore the presence of e-p coupling below T_K (Appendix B), the Allen approach is used [27]. Allen showed that e-p coupling in disordered metallic systems could be estimated by the average phonon line width over disordered wave vectors $\vec{q}$ [2,27], since the conservation rule is relaxed in the presence of disorder among different $\vec{q}$ leading to the decay of phonon into the electron-hole pair, whereby the e-p interaction is enhanced. For the ith phonon, the e-p coupling (λ) is expressed (Allen's formula),

$$\lambda = \left(\frac{\Gamma_i}{\omega^2}\right)\left(\frac{g_i}{2\pi}\right)\left(\frac{1}{N(E)}\right), \tag{4}$$

where g_i is the degeneracy of ith mode and $N(E)$ is the density of states (DOS) at the Fermi level per spin per molecule [27]. We can assume that the change in DOS remains moderate down to T_V because DOS are known to be reasonably static, as inferred from INS [25] and photoemission experiments [28]. Below T_V, $\sim$15–20% changes occur in DOS [28]. Consequently, the pellucid aspect of the e-p coupling strength is better estimated by the convolution of $\lambda N(E)$ around T_V, which is plotted in Fig. 5 for both modes. In these modes, the e-p coupling strength is absent above $\sim T_K$ on account of anharmonic effects. Whereas the moderate rise in $\lambda N(E)$ in A_{1g} mode observed below $\sim T_K$ is governed by electronic disorders that are associated with the e-p coupling interactions, the prominent increase in $\lambda N(E)$ in the T_{2g} mode [Fig. 5(b)], in comparison to that in A_{1g} mode [Fig. 5(a)], between 150 K and

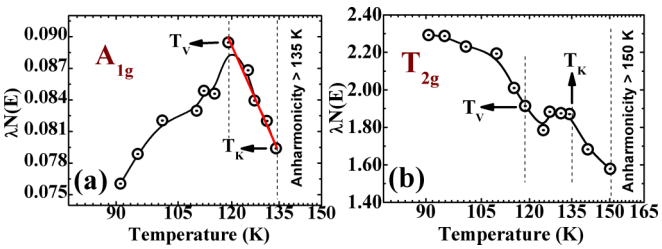

FIG. 5. (Color online) Estimated $\lambda N(E)$ for (a) A_{1g} and (b) $T_{2g}(3)$ modes.

T_V clearly affirms that the electronic states couple strongly with the T_{2g} mode. Whereas $\lambda N(E)$ remarkably remains moderate for the T_{2g} mode below T_V (down to 90 K), it steeply decreases for the A_{1g} mode, as shown in Fig. 5(a). This steep decrease of $\lambda N(E)$ is dominantly regulated by the decrease of $N(E)$ below 119 K, since λ is weakly coupled to the A_{1g} mode. However, for the T_{2g} mode, the $\lambda N(E)$ is indeed dominated by λ around T_V. Therefore, the operator Γ_5^+, which is associated with the T_{2g} mode, contributes to VT strongly compared to Γ_1^+ operator for A_{1g} mode. In the presence of strong e-p interactions, the quantum interference between the continuum of electron-hole excitations and discrete phonons leads to asymmetric Fano resonance. Therefore, the strong e-p coupling is accompanied by asymmetry in the Raman line shape [29,30]. As a result of Fano interaction, this asymmetry is incorporated in the high sensitive T_{2g} mode intensity expression as

$$I(\omega) = S\frac{\left[q + \frac{2(\omega-\omega_0)}{\Gamma}\right]^2}{\left[1 + \left(\frac{2(\omega-\omega_0)}{\Gamma}\right)^2\right]}, \tag{5}$$

where S is a constant and $|q|$ is Fano asymmetric parameter, a measure of Fano interactions and its low value implies strong e-p interaction [30].

The Raman spectra of $T_{2g}(3)$ mode is fitted with the Fano function [Eq. (5)] below $\sim T_K$ and down to structural transition T_V. Figure 6 only shows the Fano function fitted Raman profile at a few representative temperatures. The observed fitted line-shape parameters are nearly similar, as measured by Gaussian and Lorentzian convolution functions. The estimated values of $|q|$ are shown in Fig. 7(a). The increase in $1/|q|$ on cooling below 150 K clearly strengthens the presence of strong e-p coupling in T_{2g} line-shape parameters. This strong e-p coupling could be expected by two possible mechanisms: (i) the charge ordering below $\sim T_K$ has a higher correlation length than the lattice-distortion fluctuations [4] because of which it couples strongly to lattice vibration modes below T_K to evolve strong e-p coupling thereby stabilizing CO [10,11], and (ii) spin-dependent e-p interactions due to spin reorientation at T_K. To enlighten the spin-dependent e-p interactions, the Guntherodt *et al.* [31] approach is used. Within this approach, the spin-dependent electron-phonon interaction is described by the following Hamiltonian as

$$H_{EP} = \sum_{\vec{g}_m}\sum_{\vec{q}\lambda} Q_{\vec{q}\lambda}(t)\varepsilon_{-\vec{g}_m}(\vec{q}\lambda)\delta(\vec{q} - \vec{g}_m), \tag{6}$$

where $\delta(\vec{q} - \vec{g}_m)$ is the Dirac delta function, $\vec{g}_m$ is the reciprocal magnetic lattice vector, $\vec{q}$ is the wave vector, and $\varepsilon_{-\vec{g}_m}(\vec{q}\lambda)$ is the spin-phonon coupling parameter. It may be noted that $H_{EP} \neq 0$ only if (i) $\vec{q} - \vec{g}_m = 0$, which is indeed the case in Fe_3O_4 wherein the magnetic ordering occurs below $\sim T_K$, and (ii) $\varepsilon_{-\vec{g}_m}(\vec{q}\lambda) \neq 0$, which is only possible if strong s-p coupling exists.

Therefore to establish the presence of spin-dependent e-p coupling below $\sim T_K$, the presence of s-p coupling needs to be demonstrated. To check the presence of s-p coupling, the temperature-dependent Raman intensity of T_{2g} mode is plotted in Fig. 7(b). It shows the linear intensity variation below 150 K. This increase in the intensity below 150 K clearly indicates the presence of s-p coupling. These s-p interactions are caused by the modulation of magnetic exchange interaction

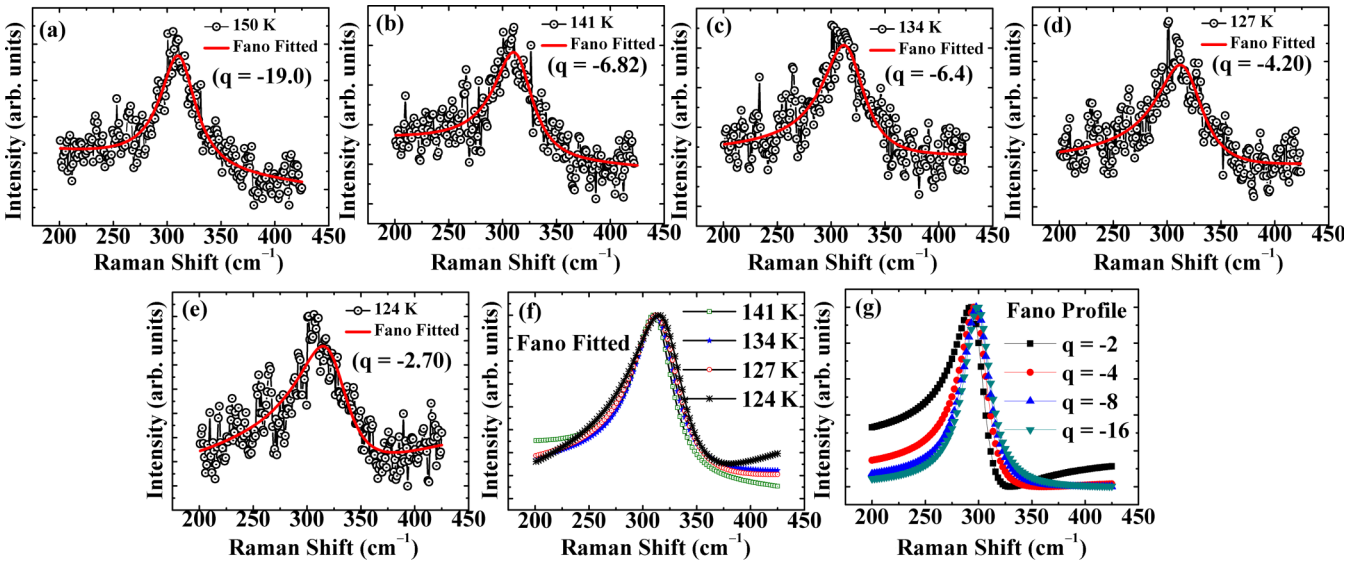

FIG. 6. (Color online) Fano function fitted Raman spectra of $T_{2g}(3)$ mode at a few representative temperatures of (a) 150 K, (b) 141 K, (c) 134 K, (d) 127 K, and (e) 124 K. (f) The Fano fitted functions at 141 K, 134 K, 127 K, and 124 K for comparison. (g) Note that the general trend of Raman line shape described by the Fano equation for different values of $|q|$ keeping ω and Γ constant; smaller the value of $|q|$ larger is the asymmetry in line shape.

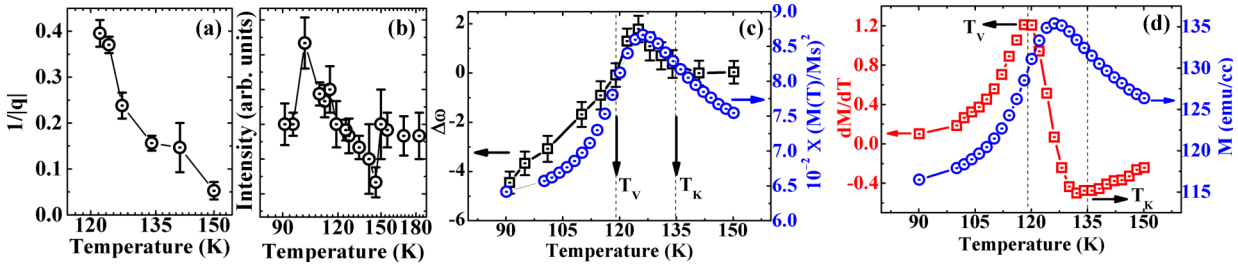

FIG. 7. (Color online) Temperature-dependent plots for T_{2g} mode highlighting T_V and T_K. (a) $1/|q|$, (b) Raman peak intensity, (c) $\Delta\omega_{s-\mathrm{phn}}(T)$ and $[\frac{M(T)}{M_S}]^2$, (d) $M(T)$ and $dM(T)/dT$ ($H = 100$ Oe, field cooling).

by lattice vibrations. It may be noted that the magnetic and structural phase transitions in highly correlated systems such as FeO, MnO, etc. are solely governed by the s-p interaction [32–34]. Further, as the bending vibrational modes minimize the effective Hamiltonian of s-p interactions [35], the T_{2g} mode, being a bending vibration mode, is therefore expected to be strongly affiliated with the s-p coupling. To further strongly establish the presence of s-p coupling, we use the Granado *et al.* [36] approach between T_K-T_V [4], according to which the Raman frequency shift of highly sensitive T_{2g} mode due to s-p contribution is expressed as $\omega(T) - \omega_0 = \Delta\omega_{s-\mathrm{phn}} \propto \langle S_i|S_j\rangle$. The term $\langle S_i|S_j\rangle$ represents the nearest-neighbor spin correlations and should vary as $[\frac{M(T)}{M_S}]^2$, where $M(T)$ is the temperature-dependent magnetization, ω_0 is the phonon frequency in absence of s-p coupling, and M_S is the saturation magnetization per Fe^{2+} ion. Hence, for the T_{2g} mode, the interdependence of the $\omega(T)$ and the s-p coupling is expressed as $\omega(T) - \omega_0 = \Delta\omega_{s-\mathrm{phn}} \propto [\frac{M(T)}{M_S}]^2$. In Fig. 7(c), the $\Delta\omega(T)$ and $[\frac{M(T)}{M_S}]^2$ curves corresponding to the T_{2g} mode are plotted simultaneously and can be seen to exhibit a maximum between T_K and T_V and also an overlap on either side of the maximum. This further provides a clear experimental evidence of the existence of strong s-p interaction in Fe_3O_4. On account of the development of a single-ion anisotropy along $\langle 100\rangle$ at T_K [4], the bending vibrations of T_{2g} mode thus couple strongly with anisotropic spin-exchange interactions and result in s-p couplings. The $M(T)$ and its derivative $\frac{dM(T)}{dT}$ of this 2D epitaxial film are also plotted in Fig. 7(d) for the pellucid view of the characteristic changes taking place near T_K and T_V. Therefore, above discussion concludes that the anomalous line-shape parameters below $\sim T_K$ to T_V are due to the strong presence of spin-dependent e-p and s-p coupling.

However, below T_V, the line-width broadening of the T_{2g} mode [Fig. 4(b)] could also be in part due to the superposition of the nearly degenerate T_{2g} modes (i.e., B_{1g}, B_{2g}, and B_{3g}), which are found below T_V. Though we do not have Raman data at lower T, these latter modes are expected to be distinguishable below 90 K since the structural transition to monoclinic phase gets complete by ~90 K, which was earlier established via the field-cooled $M(T)$ response of this sample [Fig. 5(c) of Ref. 5]. The $\omega(T)$ behavior (Fig. 4) in the structural transition regime (T_V to 90 K) of both modes could be explained by considering the magnetically frustrated spin exchange interactions, which are expected to be present in this magnetically frustrated regime. Therefore, $\omega(T)$ can be expressed by

$$\omega - \omega_0 \propto (R_2 - R_1)\langle S_i|S_j\rangle, \qquad (7)$$

where the exchange integral constants R_1 and R_2, respectively, affiliate with ferromagnetic and AF nearest neighbors since magnetic properties are determined dominantly by the exchange interactions [24,37]. The direct exchange coupling is ignored in this model. The distinct softening of $\omega(T)$ corresponding to the T_{2g} mode observed below T_V [Fig. 4(b)] could be governed by the ferromagnetic near-neighbor exchange interaction along the octahedral-oxygen-octahedral (or tetrahedral) chains. Therefore, below T_V, the $(R_2 - R_1)$ becomes more negative and leads to the softening of $\omega(T)$. The marginal hardening of $\omega(T)$ occurring below T_V in the A_{1g} mode [Fig. 4(a)] is attributed to the strong AF super-exchange interactions along the octahedral-oxygen-tetrahedral chains via the increase in $(R_2 - R_1)$, consistent with structural transformation [38]. Analogous s-p exchange interactions have also been shown in $Eu_{1-x}Y_xMnO_3$ and multiferroic manganese perovskites systems [39]. Thus, the low temperature Raman measurements on our 2D epitaxial films clearly indicate that T_K seems to be linked to the onset of strong s-p and e-p couplings. These couplings are anticipated to play a fundamental role in the occurrence of VT via the CO stabilization and band-gap opening at the Femi level in the vicinity of transition [4,10,11].

IV. CONCLUSION

In conclusion, the presence of phonon anharmonicity and strong s-p and e-p coupling are demonstrated using low temperature Raman measurements performed on a 2D epitaxial Fe_3O_4 thin film. Phonon anharmonicity dominates only down to $\sim T_K$, and below it phonons couple strongly to electron charge and spin degrees of freedom to stabilize the CO, which might be associated with spin reorientation taking place around T_K leading to the monoclinic distortions of lower symmetry. The spin reorientation at T_K induces the s-p coupling, and these couplings are responsible for the creation of strong e-p interactions below T_K. Therefore, these e-p interactions are pivotal to govern the VT. However, Raman line-shape parameters in structural transition regime (below T_V to 90 K) are governed by the e-p coupling and frustrated s-p exchange interactions. The close association of s-p interaction with MI transition in magnetic systems can also have significant prospective for spintronic applications.

APPENDIX A

To get the precise value of Raman line-shape parameters Raman data was fitted to purely Gaussian, to

purely Lorentzian, and to the convolution (multiplication) of Gaussian and Lorentzian with different background subtractions. The value of $\Sigma\chi^2$ was significantly small for the case of convolution function. Furthermore, the errors in the various fitted parameters were also a minimum in comparison to the case of fitting using purely Gaussian and/or Lorentzian functions. Regarding background subtraction, second-order polynomial and linear functions provided the nearly same fitting parameters. However, the polynomial background subtraction with average end point data correction minimized the value of $\Sigma\chi^2$ for better fitting and also discernibly retained the Fano asymmetry below 135 K. The details of these fittings are shown in Fig. 8 employing the Gaussian, Lorentzian, and Gaussian × Lorentz (multiplication) fitted Raman data at two representative temperatures of 150 and 91 K.

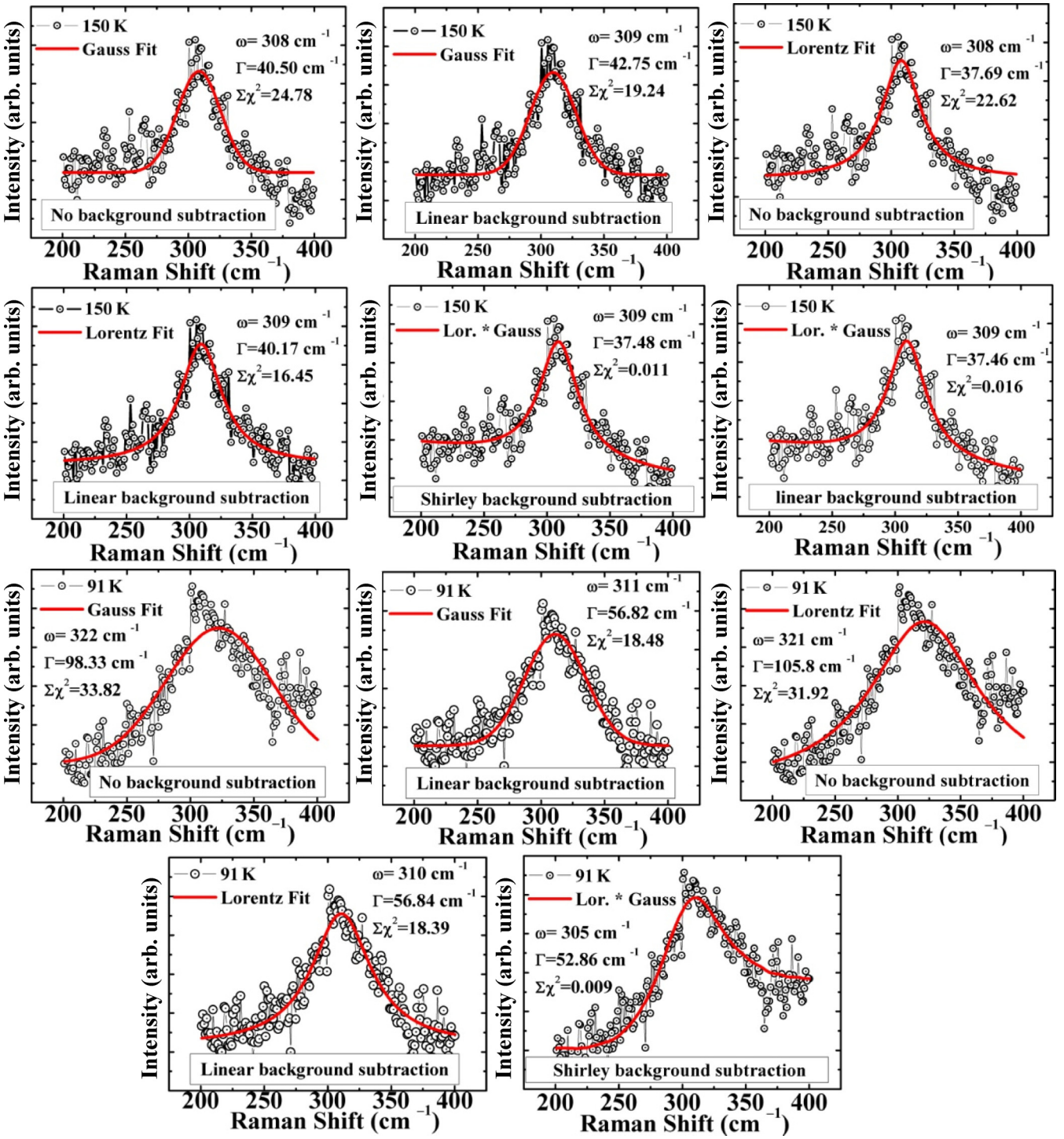

FIG. 8. (Color online) Fitting of Raman spectra corresponding to $T_{2g}(3)$ mode using different functions [Gaussian, Lorentzian, and Gaussian × Lorentzian (i.e., multiplication)] and different background subtractions (linear, Shirley, or no background subtraction) at 150 K and 91 K.

APPENDIX B

When e-p coupling is strong, formation of small polarons is expected. A general characteristic property of small polarons is the exponential renormalization of mass, $m^*_\alpha \propto \exp(\frac{\lambda\gamma_\alpha}{\bar{\omega}})$. Therefore, the mass anisotropy, $\frac{m^*_\alpha}{m^*_\beta} \propto \exp[\frac{(\gamma_\alpha-\gamma_\beta)}{\bar{\omega}}\lambda]$ is an exponential function of λ, where γ_α and γ_β are the numerical coefficients and α and β are direction cosines, respectively, and $\bar{\omega}$ is a dimensionless phonon frequency [40]. Since the presence of strong e-p coupling is observed in the 150 to T_V range in our Fe_3O_4 film; therefore, as per the above relation, mass anisotropy is expected to be present in this temperature range. The increase in mass anisotropy in presence of small polarons below 150 K had earlier been reported in epitaxial Fe_3O_4 thin films [8,41]. This interdependence of mass anisotropy and λ thus also supports the presence of strong e-p coupling below 150 K.

The resistivity (ρ) vs temperature (T) behavior of a 2D epitaxial Fe_3O_4 film deposited on a 7-nm epitaxial TiN buffered Si(100) substrate is shown in Fig. 9. The steep rise of resistivity at 119 (T_V) is clearly seen in this plot and is typical of VT.

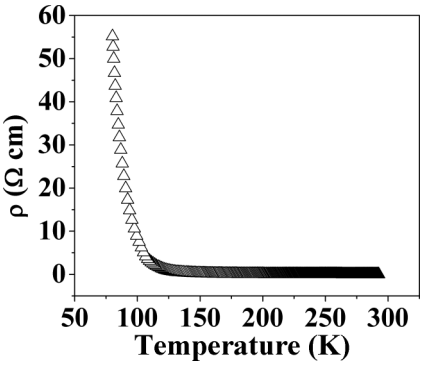

FIG. 9. Resistivity versus temperature behavior of 2D epitaxial Fe_3O_4 film showing sharp Verwey transition.

[1] Z. Zhang and S. Satpathy, Phys. Rev. B **44**, 13319 (1991).
[2] J. L. Verble, Phys. Rev. B **9**, 5236 (1974).
[3] A. R. Muxworthy and E. McClelland, Geophys. J. Int. **140**, 101 (2000).
[4] J. E. Lorenzo, C. Mazzoli, N. Jaouen, C. Detlefs, D. Mannix, S. Grenier, Y. Joly, and C. Marin, Phys. Rev. Lett. **101**, 226401 (2008).
[5] A. Kumar, D. K. Pandya, and S. Chaudhary, Appl. Phys. Lett. **102**, 152406 (2013).
[6] E. J. W. Verwey, Nature (London) **144**, 327 (1941).
[7] P. W. Anderson, Phys. Rev. **102**, 1008 (1956).
[8] D. Ihle and B. Lorenz, J. Phys. C **19**, 5239 (1986).
[9] H. T. Jeng, G. Y. Guo, and D. J. Huang, Phys. Rev. B **74**, 195115 (2006).
[10] P. Piekarz, K. Parlinski, and A. M. Oles, Phys. Rev. Lett. **97**, 156402 (2006); Phys. Rev. B **76**, 165124 (2007).
[11] M. Hoesch, P. Piekarz, A. Bosak, M. Le Tacon, M. Krisch, A. Kozłowski, A. M. Oles, and K. Parlinski, Phys. Rev. Lett. **110**, 207204 (2013).
[12] L. Degiorgi, I. Blatter-Mörke, and P. Wachter, Phys. Rev. B **35**, 5421 (1987).
[13] L. V. Gasparov, D. B. Tanner, D. B. Romero, H. Berger, G. Margaritondo, and L. Forró, Phys. Rev. B **62**, 7939 (2000).
[14] R. Gupta, A. K. Sood, P. Metcalf, and J. M. Honig, Phys. Rev. B **65**, 104430 (2002).
[15] M. Baghaie Yazdi, K.-Y. Choi, D. Wulferding, P. Lemmens, and L. Alff, New J. Phys. **15**, 103032 (2013).
[16] D. T. Margulies, F. T. Parker, M. L. Rudee, F. E. Spada, J. N. Chapman, P. R. Aitchison, and A. E. Berkowitz, Phys. Rev. Lett. **79**, 5162 (1997).
[17] J. B. Moussy, S. Gota, A. Bataille, M. J. Guittet, M. Gautier-Soyer, F. Delille, B. Dieny, F. Ott, T. D. Doan, P. Warin, P. Bayle-Guillemaud, C. Gatel, and E. Snoeck, Phys. Rev. B **70**, 174448 (2004).
[18] D. J. Evans and S. Ushioda, Phys. Rev. B **9**, 1638 (1974).
[19] R. J. McQueeney, M. Yethiraj, W. Montfrooij, J. S. Gardner, P. Metcalf, and J. M. Honig, Physica B **385-386**, 75 (2006); R. J. McQueeney, M. Yethiraj, W. Montfrooij, J. S. Gardner, P. Metcalf, and J. M. Honig, Phys. Rev. B **73**, 174409 (2006).
[20] C. H. Chio, S. K. Sharma, and D. W. Muenow, Amer. Miner. **89**, 390 (2004).
[21] S. K. Sharma, Vib. Spectra Struc. **17B**, 513 (1989).
[22] R. D. Waldron, Phys. Rev. **99**, 1727 (1955).
[23] J. R. Fuertes, S. L. Moreno, D. Errandonea, J. P. Porres, R. L. Perales, A. Segura, P. R. Hernandez, A. Munoz, A. H. Romero, and J. Gonzales, J. Appl. Phys. **107**, 083506 (2010).
[24] M. Maczka, M. Ptak, K. Hermanowicz, A. Majchrowski, A. Pikul, and J. Hanuza, Phys. Rev. B **83**, 174439 (2011).
[25] B. Handke, A. Kozłowski, K. Parliński, J. Przewoźnik, T. Ślęzak, A. I. Chumakov, L. Niesen, Z. Kąkol, and J. Korecki, Phys. Rev. B **71**, 144301 (2005).
[26] M. Balkanski, R. F. Wallis, and E. Haro, Phys. Rev. B **28**, 1928 (1983).
[27] P. B. Allen, Solid State Commun. **14**, 937 (1974).
[28] A. Chainani, T. Yokoya, T. Morimoto, and T. Takahashi, and S. Todo, Phys. Rev. B **51**, 17976 (1995).
[29] U. Fano, Phys. Rev. **124**, 1866 (1961).
[30] K. H. Kim, J. Y. Gu, H. S. Choi, D. J. Eom, and T. W. Noh, J. Korean Phys. Soc. **31**, 197 (1997).
[31] G. Guntherodt, W. Bauhofer, and G. Benedek, Phys. Rev. Lett. **43**, 1427 (1979).
[32] D. Schrupp, M. Sing, M. Tsunekawa, H. Fujiwara, S. Kasai, A. Sekiyama, S. Suga, T. Muro, V. A. M. Brabers, and R. Claessen, Europhys. Lett. **70**, 789 (2005).
[33] Ch. Kant, F. Mayr, T. Rudolf, M. Schmidt, F. Schrettle, J. Deisenhofer, and A. Loidl, Eur. Phys. J. Special Topics **180**, 43 (2009).

[34] D. J. Lockwood and M. G. Cottam, J. Appl. Phys. **64**, 5876 (1988).
[35] D. L. Bergman, R. Shindou, G. A. Fiete, and L. Balents, Phys. Rev. B **74**, 134409 (2006).
[36] E. Granado, A. García, J. A. Sanjurjo, C. Rettori, I. Torriani, F. Prado, R. D. Sánchez, A. Caneiro, and S. B. Oseroff, Phys. Rev. B **60**, 11879 (1999).
[37] W. Baltensperger and J. S. Helman, Helvetica Physica Acta **41**, 668 (1968).
[38] M. R. Senn, J. P. Wright, and J. P. Attfield, Nature (London) **481**, 173 (2011); A. D. Rowan, C. H. Patterson, and L. V. Gasparov, Phys. Rev. B **79**, 205103 (2009).
[39] J. A. Moreira, A. Almeida, W. S. Ferreira, J. E. Araújo, A. M. Pereira, M. R. Chaves, J. Kreisel, S. M. F. Vilela, and P. B. Tavares, Phys. Rev. B **81**, 054447 (2010).
[40] P. E. Kornilovitch, Phys. Rev. B **59**, 13531 (1999).
[41] R. Ramos, S. K. Arora, and I. V. Shvets, Phys. Rev. B **78**, 214402 (2008).